JOURNAL OF QUATERNARY SCIENCE (2020) 1–13 ISSN 0267-8179. DOI: 10.1002/jqs.3177

JQS Journal of Quaternary Science QRA Quaternary Research Association

Fingerprinting the Late Pleistocene tephras of Ciomadul volcano, eastern–central Europe

SZABOLCS HARANGI,[1,2]* KATA MOLNÁR,[2,3] AXEL K. SCHMITT,[4] ISTVÁN DUNKL,[5] IOAN SEGHEDI,[6] ÁGNES NOVOTHNY,[7] MIHÁLY MOLNÁR,[3] BALÁZS KISS,[1] THEODOROS NTAFLOS,[8] PAUL R. D. MASON[9] and RÉKA LUKÁCS[1]

[1]MTA-ELTE Volcanology Research Group, Pázmány Péter Stny. 1/C, Budapest, H-1117, Hungary
[2]Department of Petrology and Geochemistry, Eötvös Loránd University, Pázmány Péter Stny. 1/C, Budapest, H-1117, Hungary
[3]Isotope Climatology and Environmental Research Centre, Institute for Nuclear Research, Hungarian Academy of Sciences, Bem Tér 18/C, Debrecen, H-4026, Hungary
[4]Institute of Earth Sciences, Universität Heidelberg, Im Neuenheimer Feld 234-236, Heidelberg, 69120, Germany
[5]Sedimentology and Environmental Geology, Geoscience Centre, Georg-August Universität Göttingen, Goldschmidtstraße 3, Göttingen, 37077, Germany
[6]Institute of Geodynamics, Romanian Academy, 19-21 Jean-Louis Calderon Street, Bucharest, R-020032-37, Romania
[7]Department of Physical Geography, Eötvös Loránd University, Pázmány Péter Stny. 1/C, Budapest, H-1117, Hungary
[8]Department of Lithospheric Research, University of Vienna, Althanstraße 14, Vienna, A-1090, Austria
[9]Department of Earth Sciences, Utrecht University, Budapestlaan 4, Utrecht, 3584 CD, The Netherlands

Received 10 May 2019; Revised 28 November 2019; Accepted 29 November 2019

ABSTRACT: Late Pleistocene tephras derived by large explosive volcanic eruptions are widespread in the Mediterranean and surrounding areas. They are important isochronous markers in stratigraphic sections and therefore it is important to constrain their sources. We report here tephrochronology results using multiple criteria to characterize the volcanic products of the Late Pleistocene Ciomadul volcano in eastern–central Europe. This dacitic volcano had an explosive eruption stage between 57 and 30 ka. The specific petrological character (ash texture, occurrence of plagioclase and amphibole phenocrysts and their compositions), the high-K calc-alkaline major element composition and particularly the distinct trace element characteristics provide a strong fingerprint of the Ciomadul volcano. This can be used for correlating tephra and cryptotephra occurrences within this timeframe. Remarkably, during this period several volcanic eruptions produced tephras with similar glass major element composition. However, they differ from Ciomadul tephras by glass trace element abundances, ratios of strongly incompatible trace elements and their mineral cargo that serve as discrimination tools. We used (U-Th)/He zircon dates combined with U-Th in situ rim dates along with luminescence and radiocarbon dating to constrain the age of the explosive eruptions of Ciomadul that yielded distal tephra layers but lack of identified proximal deposits.

KEYWORDS: Ciomadul volcano; distal tephra; petrochemical fingerprint; tephrochronology; (U-Th)/He zircon dating

Introduction

Tephra layers in terrestrial sediments are often used as key horizons in Quaternary sections because they provide isochronous markers and therefore are a fundamental tool for correlating distant occurrences and yielding absolute age constraints (Lowe, 2011). These are important in various fields, such as palaeoclimatic, palaeoenvironmental and archaeological research. In addition, identifying distal tephra deposits and their sources can reveal the long-term eruptive behaviour of volcanoes, particularly documenting their potential for large explosive eruptions. The recognition of cryptotephras in many geological archives has further expanded this approach (Blockley *et al.*, 2005; Davies, 2015). Although there has been significant progress in the documentation of tephra and cryptotephra layers, correlation with proximal equivalents is not always straightforward and the source volcanoes often remain elusive. Thus, along with an emerging comprehensive tephra database from distal locations, there is also a need for proper knowledge of the potential volcanic sources, i.e. fingerprinting deposits proximal to their sources to characterize tephra-producing volcanoes (Tomlinson *et al.*, 2015).

Tephra correlation is usually based on the major element composition of glass shards and the known eruption age of the source volcano. However, major element compositions of evolved magmas are often similar and therefore trace element data are crucial, as demonstrated by several studies since the advance of laser-ablation inductively coupled plasma mass spectrometry (LA-ICP-MS; Pearce *et al.*, 1999, 2007; Harangi *et al.*, 2005; Tomlinson *et al.*, 2010). Characterization of a volcanic product can also involve major mineral contents and compositions, as well as glass shard morphology (e.g. de Silva and Francis, 1989; Shane *et al.*, 2003; Harangi *et al.*, 2005; Bosio *et al.*, 2019). Geochronology also has an important role in such studies, as accurate age constraints are important both for the proximal volcanic deposits and its distal fall out. However, dating Quaternary volcanic eruptions is often problematic, particularly because available methods cannot be applied to all materials. Zircon (U-Th)/He dating has

*Correspondence: Szabolcs Harangi, MTA-ELTE Volcanology Research Group, as above.
E-mail: szabolcs.harangi@geology.elte.hu

become a promising technique for calc-alkaline felsic tephras, which typically contain zircon (Schmitt *et al.*, 2006, 2010; Danišík *et al.*, 2012, 2017; Harangi *et al.*, 2015; Molnár *et al.*, 2018, 2019), but not necessarily K-feldspar so that Ar-Ar dating cannot be applied. Other methods (e.g. ^{14}C, or luminescence methods) have upper age limits, and also rely on the often fortuitous presence of suitable materials.

A large number of Quaternary volcanoes in and around the Mediterranean area have frequently erupted explosively and deposited widespread tephra beds in this region (Fig. 1; e.g. Tomlinson *et al.*, 2012a,b, 2015; Wulf *et al.*, 2018). They are located in central and southern Italy, Greece and Anatolia, whereas an additional potential volcanic source was only recently recognized in the southeastern Carpathians, Romania, i.e. the late Pleistocene Ciomadul volcano (Harangi *et al.*, 2015; Szakács *et al.*, 2015; Karátson *et al.*, 2016; Molnár *et al.*, 2018, 2019). Tephra beds in the Black Sea drilling cores (Cullen *et al.*, 2014), in loess deposits of Ukraine (Wulf *et al.*, 2016) and in Middle Palaeolithic caves (Veres *et al.*, 2018) have been recently suggested as derived from large explosive eruption events of Ciomadul volcano. However, to confirm this and to elucidate the regional impact of the Ciomadul eruptions, a better characterization of the Ciomadul tephras is necessary through geochronological, petrological and geochemical fingerprinting to constrain the accurate age and the nature of the volcanic products. We discuss also the limits of such data in tephrochronology.

Geological background

Ciomadul is the youngest volcano of the Carpathian–Pannonian Region (Fig. 2) in eastern–central Europe. It formed over the last 1 Myr with its last eruptions at around 30 ka (Vinkler *et al.*, 2007; Harangi *et al.*, 2010, 2015; Szakács *et al.*, 2015; Karátson *et al.*, 2016, 2019; Molnár *et al.*, 2018, 2019; Lahitte *et al.*, 2019). It is a volcanic complex, where volcanism started with intermittent lava dome extrusion events (1000–300 ka; Molnár *et al.*, 2018). This was followed by development of the more voluminous Ciomadul volcanic complex (160–30 ka; Harangi *et al.*, 2015; Karátson *et al.*, 2016, 2019; Molnár *et al.*, 2019), an amalgamation of several lava domes truncated by two deep explosion craters (Sft Ana and Mohos, respectively). Explosive eruptions characterized only the youngest eruptive epoch, which lasted from 57 to 30 ka (Harangi *et al.*, 2015; Molnár *et al.*, 2019). This explosive volcanic activity involved moderate to large Vulcanian, subplinian to Plinian and phreatomagmatic eruptions (Szakács *et al.*, 2015; Karátson *et al.*, 2016), which occasionally resulted in far-reaching tephras (Vinkler *et al.*, 2007; Harangi *et al.*, 2015; Karátson *et al.*, 2016; Wulf *et al.*, 2016; Veres *et al.*, 2018). Volcanological features of the explosive volcanic products (both proximal and medial–distal) were described by Vinkler *et al.* (2007), Karátson *et al.* (2016) and Molnár *et al.* (2019). Based on the major element composition of the glasses, Vinkler *et al.* (2007) and Harangi *et al.* (2010) defined two compositionally distinct groups (Tuşnad-type and Bixad-type; represented by the 50-ka pumices from a pyroclastic fall deposit found near Băile Tuşnad and 32-ka pumice from a pyroclastic flow deposit at the Bixad locality, respectively; these are denoted as BTS-1.3 and BIX-1.2 by Karátson *et al.*, 2016; Figures 2 and 3A). This is consistent with the bimodal character of pumice and lava dome samples from the latest (i.e. <57 ka) Ciomadul activity (Fig. 3B) suggesting the existence of two main erupted magma types. Karátson *et al.* (2016) published a larger glass data set, which involved more localities and this confirmed the two compositional groups (Fig. 3A). However, they interpreted the

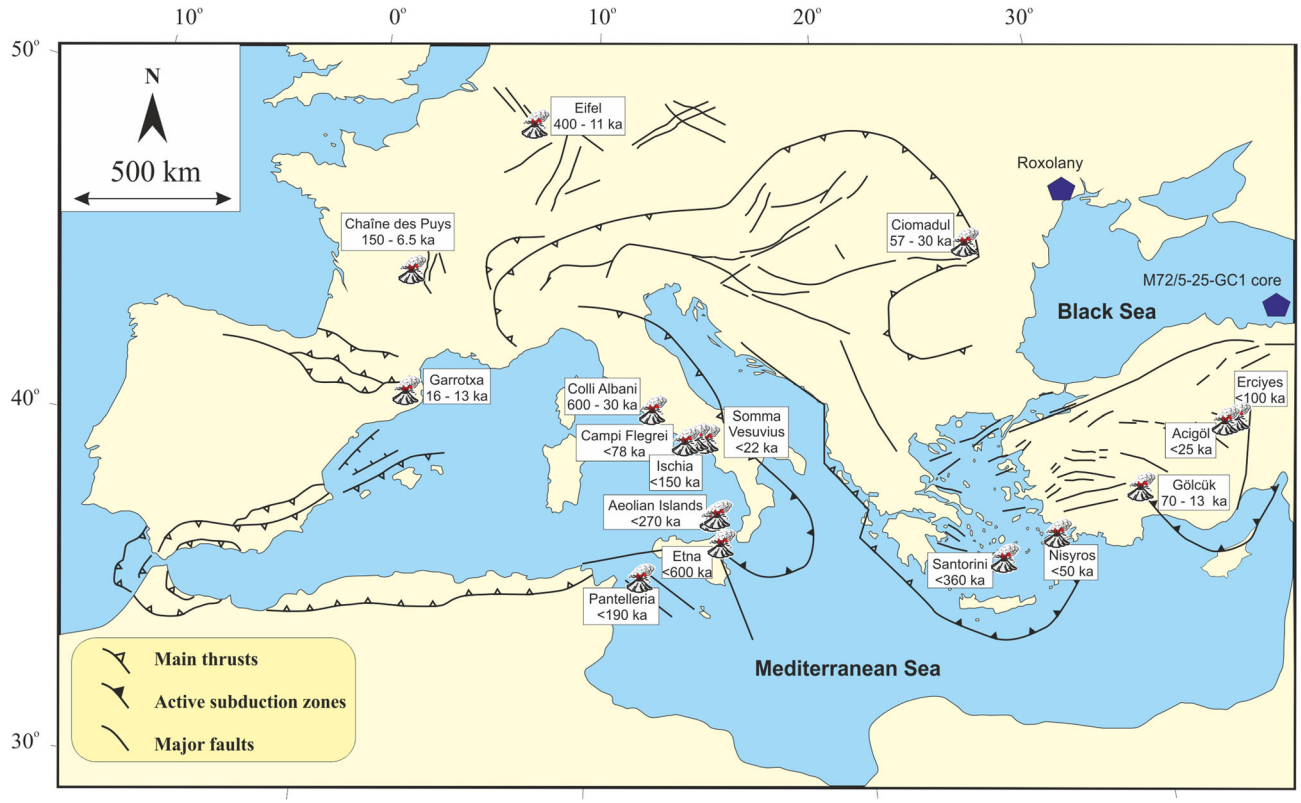

Figure 1. Volcanoes in and around the Mediterranean region that produced large explosive eruptions resulting in deposition of far-reaching distal tephra for the last 100 kyr (references are in Supporting Material_1). Roxolany (Wulf *et al.*, 2016) and drill sites in the southern Black Sea (Cullen *et al.*, 2014) are shown where distal tephra of Ciomadul origin was assumed. For Ciomadul only the latest, dominantly explosive volcanic epoch is shown (Harangi *et al.*, 2015; Molnár *et al.*, 2019). [Color figure can be viewed at wileyonlinelibrary.com]

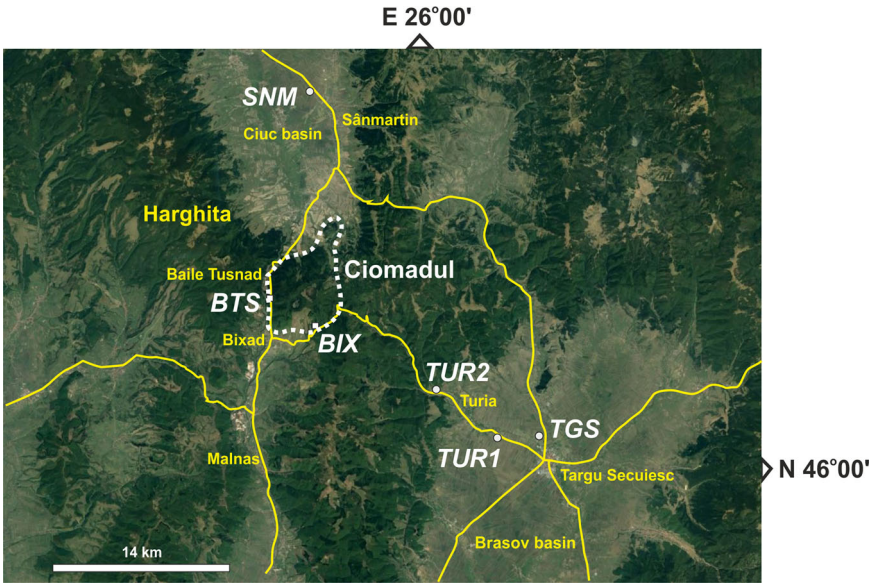

Figure 2. Location of the Ciomadul volcanic complex (dotted line) at the south-easternmost edge of the Pliocene to Quaternary Harghita volcanic chain and the locations of distal tephras (SNM, TUR1 and TUR2, TGS) recognized at 20–25 km distance around the volcano. The localities of BTS (Tușnad) and BIX (Bixad) tephras are two proximal occurrences representing two main compositional types of pumices and glasses within the Ciomadul tephras (Vinkler *et al.*, 2007; Harangi *et al.*, 2010; Karátson *et al.*, 2016). Yellow lines are main roads. [Color figure can be viewed at wileyonlinelibrary.com]

major element compositional trend of glasses to reflect a temporal evolution of magma differentiation, i.e. a highly evolved EPPA (Early Phreatomagmatic and Plinian Activity) magma type was superseded by a less evolved MPA (Middle Plinian Activity) magma and, finally, the youngest eruptions reverted to slightly more evolved LSPA (Latest St. Ana Phreatomagmatic Activity) magma composition. Their LSPA glass group shows a larger scatter than MPA and EPPA glasses, although most of them have Tușnad affinity.

Distal tephras around Ciomadul and analytical techniques

Distal tephra deposits (i.e. tephra layers found far from the volcanic edifice usually embedded in non-volcanic sedimentary sequences) provide unique opportunities to record relatively large eruption events. Around the Ciomadul volcanic complex (Vinkler *et al.*, 2007; Harangi *et al.*, 2015; Karátson *et al.*, 2016) such volcanic layers have been identified at distances ~20–25 km from the vent (Fig. 2). We use the tephra names as described by Karátson *et al.* (2016) for clarity. North-west of Sânmartin (Csíkszentmárton, lower Ciuc or Csíki basin), a well-preserved tephra bed is found within a Pleistocene gravely sequence (SNM tephra). South-east of Ciomadul two distinct tephra units (TUR and TGS tephras) occur in Pleistocene fluvial–alluvial basin-filling deposits. They are found at three localities north-west and south of Turia (Torja; TUR1 and TUR2) and north-west of Târgu Secuiesc (Kézdivásárhely) in the NE Brasov (Háromszéki) basin (Fig. 2). Description of the studied outcrops is presented in Supporting Material_2. Although volcanological features and glass compositions have been reported for these tephras (Vinkler *et al.*, 2007; Karátson *et al.*, 2016), petrological characteristics and eruption ages are unknown or controversial (Harangi *et al.*, 2015; Karátson *et al.*, 2016). Geochemical data from the literature are here evaluated, including data for the proximal tephra deposits, among which those from Tușnad (BTS) and Bixad (BIX) are of particular interest as they were suggested as type localities for two distinct glass compositional groups. These data were complemented by petrological and geochronological analyses to fingerprint the Ciomadul volcanic products.

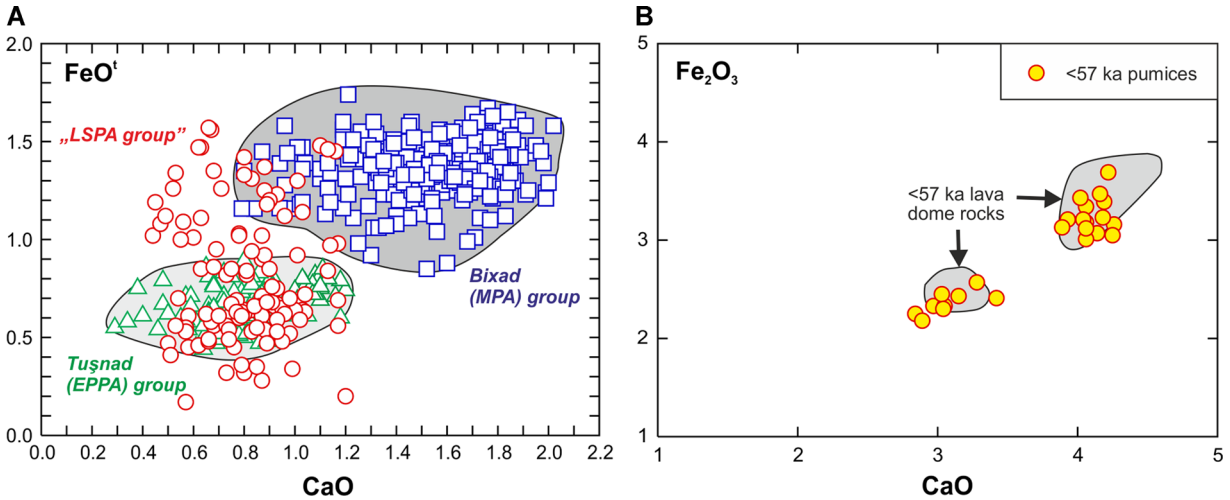

Figure 3. A. Glass major element data (in wt %; FeO^t is total iron expressed as FeO; Vinkler *et al.*, 2007; Karátson *et al.*, 2016; this study and unpublished data) for the explosive volcanic products of Ciomadul. Vinkler *et al.* (2007) defined two groups (Bixad and Tușnad), whereas Karátson *et al.* (2016) distinguished three compositional groups, where their EPPA (Early Phreatomagmatic and Plinian Activity) is the equivalent of the Tușnad group, whereas their MPA (Middle Plinian Activity) group is the equivalent of the Bixad group. Note that most of their LSPA (Late St. Ana Phreatomagmatic Activity) group tephras fall into the Tușnad group. Because the EPPA, MPA and LSPA abbreviations imply successive volcanic activity, we prefer the group names given by Vinkler *et al.* (2007). B. Bulk rock composition of proximal pumices (SM_Table 1) and the <57-ka lava dome rocks (Molnár *et al.*, 2019). They also form two compositional groups similar to the glass data. [Color figure can be viewed at wileyonlinelibrary.com]

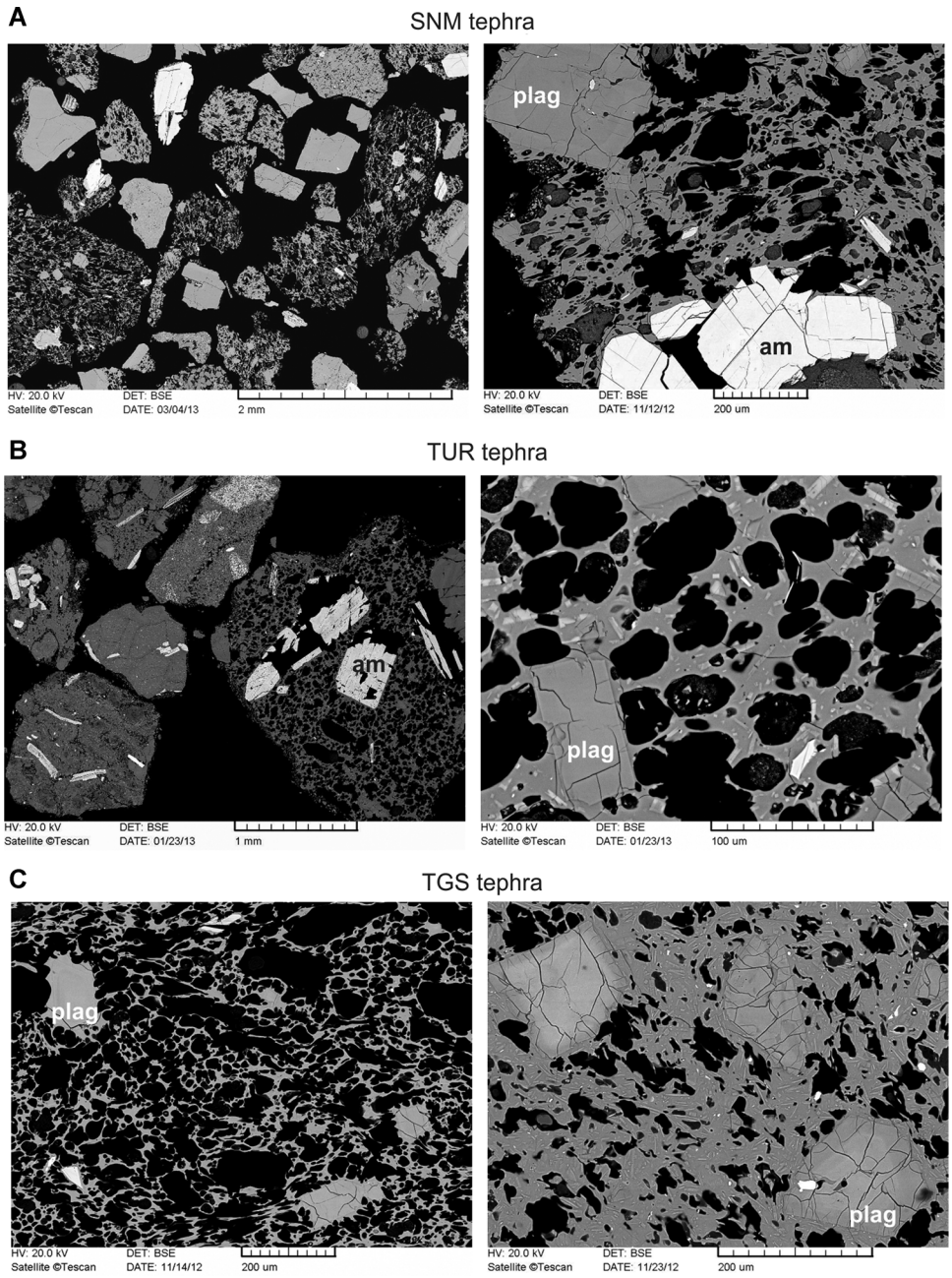

Figure 4. Textural characteristics of the volcanic ash fragments of the studied Ciomadul tephras: micropumice and dense lithic ash grains in the SNM (A) and TUR tephra (B). Closer views of micropumice with plagioclase (plag) and amphibole (am) phenocrysts are given at the right side. Note the microlite content of the glassy groundmass. Two textural types of the pumices from the TGS tephra (C): light, strongly vesicular pumice (left) and dense microlite-bearing grey pumice (right) with plagioclase phenocrysts.

Samples from the distal localities were collected for geochronological, petrological and geochemical analysis. Eruption ages of the tephras were determined directly by combined U-Th and (U-Th)/He zircon dating as described by Harangi *et al.* (2015) and Molnár *et al.* (2018, 2019) and indirectly by dating the underlying and overlying sediments using luminescence and radiocarbon methods. Detailed description of the analytical conditions along with the geochemical data is found in Supporting Material_1.

Results

Petrographic features

The SNM tephra comprises ash-sized pumice (micropumice) with an estimated relative volume of 70% and loose crystals (mostly plagioclase; ca. 20 vol.%) as juvenile clasts, whereas the remaining 10 vol% consists of lithic clasts, which are predominantly dense dacite fragments. Within the pumice, highly vesicular microlite-poor and less vesicular microlite-rich clasts can be distinguished (Fig. 4A). Pumice contains mostly plagioclase and amphibole phenocrysts with subordinate biotite. In contrast, the TUR ash layers contain a larger amount (ca. 70 vol.%) of dense volcanic fragments and only <5 vol.% pumice (Fig. 4B), whereas the remaining part comprises loose crystals (mostly plagioclase). The dense volcanic fragments resemble the dacitic lava dome rocks of the Ciomadul volcano (Kiss *et al.*, 2014; Molnár *et al.*, 2019). Pumice is variously vesiculated and the glass groundmass contains microlites in various amounts. Both clast types are crystal-poor (≤10 vol.%) and have the same phenocryst assemblage, i.e. plagioclase, amphibole and biotite in decreasing abundance. The accessory phases are apatite, zircon and titanite in both SNM and the TUR tephra deposits.

The TGS tephra consists of highly vesicular white and denser grey pumice clasts (altogether ca. 85 vol.%) of lapilli size.

High-resolution back-scattered electron (BSE) images revealed that they have subtle differences in their texture (Fig. 4C). The low-density white, frothy pumice clasts contain thin microlite-free glass walls and abundant vesicles, whereas the grey pumice clasts have thicker bubble walls and higher microlite content. Transitional textural types between these two end-members are also observed. These textural variations could result from tapping different parts of the conduit system during ascent and vesiculation of magma (Bouvet de Maisonneuve *et al.*, 2009). However, all the TGS pumice types have the same phenocryst assemblage: plagioclase, amphibole and biotite. In addition, these deposits contain about 15 vol.% lithic clasts, which are all cognate dacites with the same mineral content as the pumice.

Pumice clasts from the two proximal tephra localities (BTS and BIX; Fig. 2) have the same petrographic character as the TGS pumices, i.e. they contain microlite-bearing glassy groundmass and phenocrysts of plagioclase, amphibole and biotite.

Geochemistry

Bulk rock and glass compositions

Bulk rock analysis was conducted on individual pumice clasts of the two proximal locations, the distal TGS tephra and a bulk pumice sample of the SNM tephra (SM_Table 1). Bulk rock analysis of the TUR tephra was not performed due to a high abundance of lithic fragments. Chemical compositions are compared to the published proximal explosive volcanic products (Vinkler *et al.*, 2007; Molnár *et al.*, 2019; Fig. 3B). The TGS pumice clasts have uniform composition, they are high-K dacites (SiO_2 = 63–64 wt%; K_2O = 3.2–3.3 wt%; K_2O/Na_2O = 0.72–0.82, on an anhydrous basis), similar to most of the proximal explosive volcanic products of the Ciomadul volcanic complex. The elevated CaO content (6.6–8.0 wt%), which is unique in Ciomadul rocks, is due to entrapment of secondary carbonates in the vesicles, which remained even after careful ultrasonic cleaning of the pumice clasts. In contrast, the bulk micropumice sample of SNM tephra reflects a more evolved magma composition (SiO_2 = 68.9 wt%; K_2O = 3.8 wt%, K_2O/Na_2O = 0.8, on an anhydrous basis) showing some similarities to the Tuşnad (BTS) pumices. This slight compositional difference can also be observed in the trace element abundances. In general, the distal tephras have trace element abundances typical of Ciomadul proximal pumice with strong enrichment in Ba and Sr (both above 1000 p.p.m.) and depletion in the heavy rare earth elements (HREE; Yb<1.2 p.p.m.) and yttrium (Y<10 p.p.m.). The SNM micro-pumice composite sample has a slightly lower bulk trace element abundance than TGS pumice, similar to that of Tuşnad pumice.

The SNM and TUR tephras contain ash fragments with glassy groundmass and variable phenocrysts and microlites, whereas the TGS tephra contains pumice clasts with up to 30 vol.% crystal content. Crystal and/or microlite-free glass shards are absent. We analysed the glasses of the micropumices in the SNM and TUR tephras and the groundmass glass of the TGS pumices (SM_Table 2), where microlites are much less abundant. Our results overlap with or are very close to those published by Karátson *et al.* (2016) for the same localities (Supporting Material_1). Occasional small differences could be due to the heterogeneities of the ash fragments as described in the petrography section. The glasses of the distal Ciomadul tephras are rhyolitic, having 71–79 wt% SiO_2 and a high-K character (K_2O = 3.5–5.5 wt%; K_2O/Na_2O = 1.15–1.95). They form two distinct groups, one of them represented by the SNM and TUR tephras and the other involving the TGS tephras. This is illustrated by the FeO^t vs. CaO relationship (Fig. 5), a bivariate plot that was effectively used in distinguishing tephra deposits in New Zealand (Shane, 2000; Pearce *et al.*, 2008). Glass compositions of the SNM and TUR tephras fall within the Tuşnad group, whereas the TGS glasses have Bixad affinity.

In situ trace element analyses could not be performed on the distal tephras due to the small-sized ash fragments and the microlite content in the glassy groundmass. In contrast, this was successful for the glasses of the proximal Bixad (BIX) and Tuşnad (BTS) pumices (SM_Table 3). There are only subtle trace element differences between the two groups, whereby the Tuşnad glasses display slightly lower overall trace element abundances compared to the Bixad glasses. Of note, both groups have overlapping trace element abundances (except for Sr) with their respective bulk rock data (Fig. 6). The SNM bulk tephra perfectly overlaps with the Tuşnad pumices. Thus, both bulk rock and in situ glass trace element data can be effectively used to fingerprint Ciomadul tephra. The most characteristic features are the elevated Ba content and depletion of Y and HREE.

Mineral phases

The main mineral phases in Ciomadul pumice are plagioclase, amphibole and biotite in addition to minor amounts of apatite, accessory zircon and occasional titanite. Mg-rich minerals such as orthopyroxene and olivine can be found rarely within amphibole phenocrysts (Vinkler *et al.*, 2007). Plagioclase and amphibole show various internal zoning patterns implying complex open-system magma storage evolution (Kiss *et al.*, 2014). Compositions of these mineral phases (SM_Tables 4

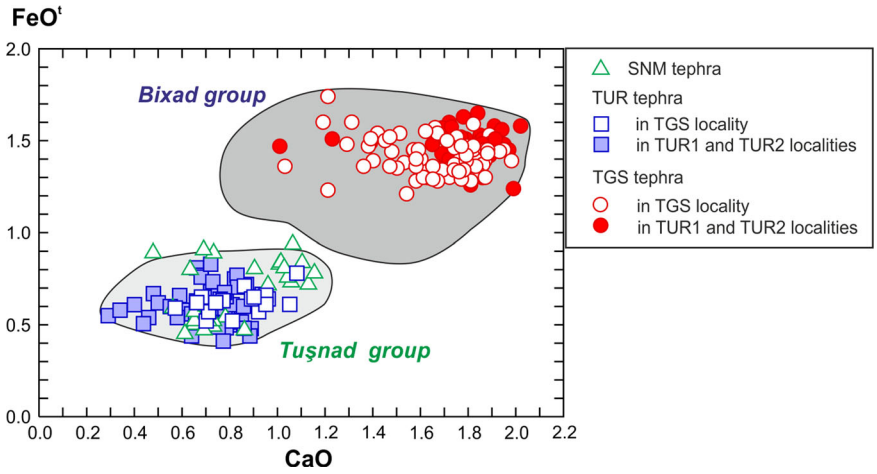

Figure 5. Glass major element compositions (wt%) of the studied distal tephra deposits. The TGS tephra has a Bixad affinity, whereas the SNM and TUR tephras fall into the Tuşnad group. Contour lines of the two compositional groups are from Fig. 3. Data: this study and Karátson *et al.* (2016). [Color figure can be viewed at wileyonlinelibrary.com]

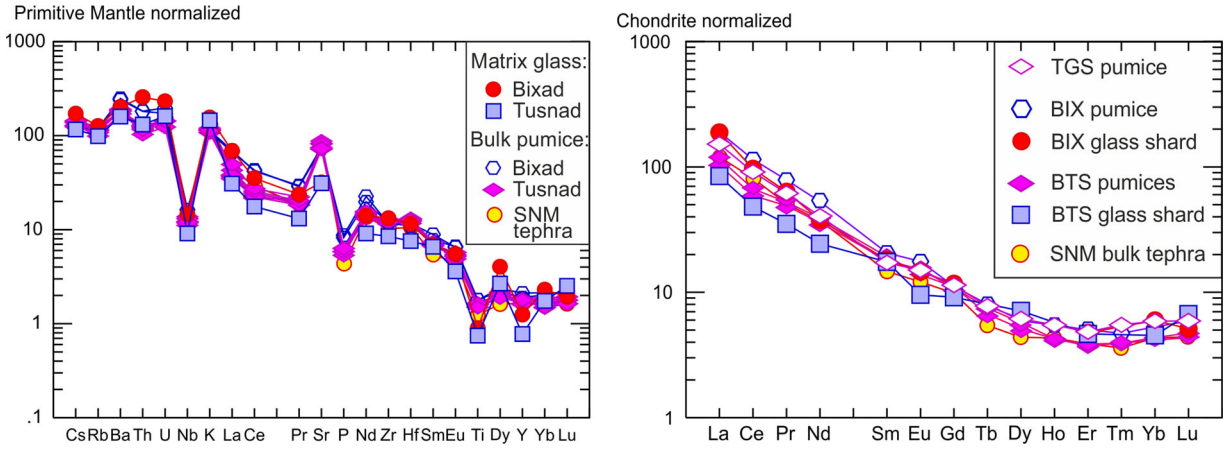

Figure 6. Primitive mantle and chondrite- (Sun and McDonough, 1989) normalized trace element and rare earth element patterns of matrix glasses and bulk pumices (Molnár *et al.*, 2019) of Ciomadul pyroclastic deposits. Note that the in situ glass and the corresponding bulk pumice trace element concentrations are indistinguishable. [Color figure can be viewed at wileyonlinelibrary.com]

and 5) show systematic differences, where the SNM and TUR tephra differs from the TGS tephra. SNM and TUR plagioclase is more sodic (An = mostly 25–35 mol%, with a minor compositional group at 45–50 mol%) and resembles Tușnad plagioclase (Fig. 7). In contrast, TGS plagioclase (An = mostly 40–50 mol%) has a Bixad affinity. The same conclusions can be drawn based on amphibole compositional data (Fig. 7). The TGS and Bixad amphiboles (pargasites) have higher Al content compared to the Tușnad-type SNM and TUR amphiboles (hornblendes).

Geochronology

Combined U-Th and (U-Th)/He ages

Accurate eruption dating is crucial in tephrochronology. The eruption history of Ciomadul volcano was constrained by single-grain zircon (U-Th)/He dating (Harangi *et al.*, 2015; Molnár *et al.*, 2018, 2019). As a result, it was shown that explosive eruptions of Ciomadul took place between 57 and 30 ka. However, controversies in the TGS tephra age and lack of data for the SNM tephra required further geochronological work. For the TGS tephra, an age of 38.9 ± 1.8 ka was proposed by Harangi *et al.* (2015), although the single-zircon dates show some heterogeneity. Therefore, further zircon grains were dated by (U-Th)/He methods and complemented by careful U-Th dating of the outermost margins of the crystals.

In the evaluation of single zircon dates (SM_Tables 6 and 7), data having high uncertainty (>10%) together with those which lie outside the 95% confidence interval (i.e. mean ± 2 SD, assuming normal/Gaussian distribution) were excluded from further calculations. Even after such data processing, the F_T-corrected (U-Th)/He single-grain zircon dates in the SNM tephra show a relatively large scatter (between 63 and 30 ka; $n = 12$; Fig. 8), whereas zircons from the TGS sample show less scattered values. In the TGS tephra, (U-Th)/He zircon dates from the white pumice fraction ('202-k') vary from 38 to 25 ka ($n = 7$), whereas data of the heavier grey pumices ('202-n') overlap with this time interval, yielding ages between 34 and 22 ka ($n = 3$). The age ranges stated above are minimum values because the samples are <350 ka and they are deficient in ^{230}Th. Thus, accurate (U-Th)/He dating requires a correction for U-series disequilibrium at the time of eruption (e.g. Farley *et al.*, 2002).

U-Th isotope spot analyses of single zircon crystals (SM_-Table 8) were conducted for disequilibrium correction calculations of the F_T-corrected (U-Th)/He dates. Both average crystallization ages and individual ages from the double-dating method were applied for the correction (see details in Danišík *et al.*, 2017 and Molnár *et al.*, 2018, 2019). For TGS tephra, the 'average crystallization age' correction method yielded an eruption age of 33.4 ± 4.2 ka ($n = 13$; goodness of fit: 0.003; average zircon crystallization age: 157 ± 10 ka), whereas the 'double-dating' method gave 29.5 ± 1.6 ka ($n = 5$; goodness of fit: 0.753; SM_Table 7, Fig. 8). These ages are younger than those determined by Harangi *et al.* (2015) based on fewer single zircon dates. For the SNM tephra, 12 zircon grains yielded F_T-corrected dates ranging between 63 ± 5 and 29.7 ± 2.2 ka (Fig. 8). This large range probably indicates an incompletely degassed zircon population due to the comparatively cold conditions of a phreatomagmatic explosive eruption. The U-Th rim ages of zircon show a range from 55.1 ± 10.5 ka up to secular equilibrium (>350 ka). A similar age range is also observed for zircon interiors. This supports our interpretation that old zircons were mixed into the erupted material. Careful evaluation of the individual zircon (U-Th)/He dates led to rejection of dates significantly older than the youngest rim age, i.e. crystallization age. As a result, only five zircons remained for the eruption age calculation yielding an error-weighted average age of 33.1 ± 8.3 ka based on a double dating method (SM_Table 7). However, its goodness of fit (3.86×10^{-8}) is well below the acceptable value (0.001) as stated in Press *et al.* (2002). At present, the most reliable (U-Th)/He zircon age is found for a single crystal which yielded an outer rim U-Th apparent age of $452 + \infty/-113$ ka. In this case, no disequilibrium age correction is required and the obtained F_T-corrected (U-Th)/He date of 29.7 ± 4.4 ka (2σ uncertainty) is tentatively considered as the most reliable eruption age estimate available.

Luminescence dating

Luminescence dating [optically stimulated lumiscence (OSL) age of quartz, post-IR infra-red stimulated luminescence (post-IR $IRSL_{290}$) age of feldspars from the same samples] of sandy sediment comprising tephra units was used to attempt bracketing the ages of the distal TGS and TUR tephras in three localities (Loc TUR1, TUR2 and TGS; SM_Table 9, Fig. 2; Supporting Material_2). For the post-IR $IRSL_{290}$ dating on feldspars, no or only negligible fading rates were detected, and therefore a fading correction was not applied. In general, the OSL and the post-IR $IRSL_{290}$ ages show good agreement except for the oldest samples, where the post-IR $IRSL_{290}$ ages significantly overestimate the corresponding OSL ages. This

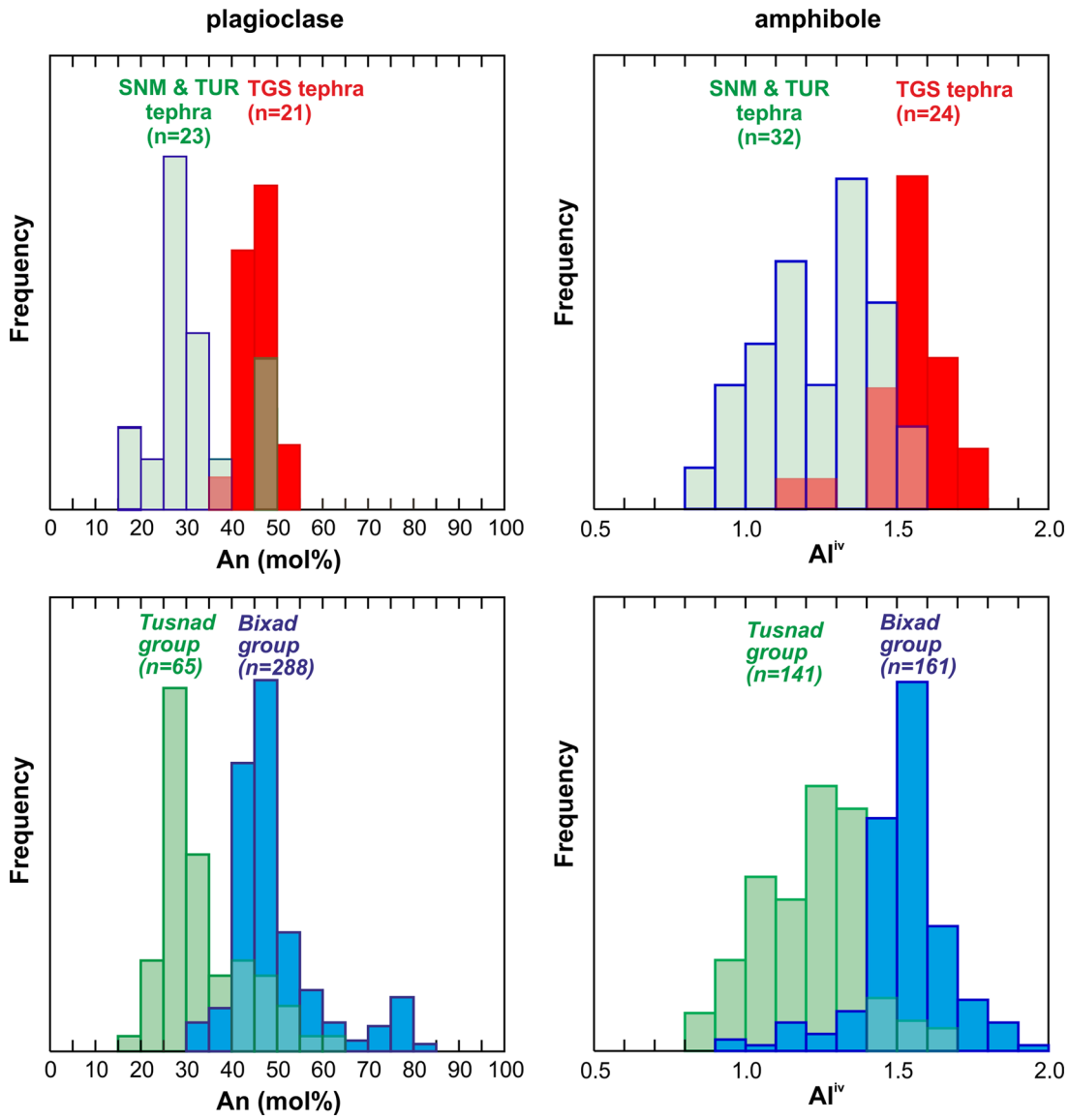

Figure 7. Compositional features of plagioclase (An end-member in mol%) and amphibole (Al^{iv} = Al in tetrahedral site in atoms per formula unit [apfu]), the main phenocrysts of the Ciomadul dacites (frequency is relative and dependent on the number of analyses *n*; plot is unscaled for *n*). The SNM and TUR tephra can be distinguished from the TGS tephra based on mineral chemistry and they show an affinity to the Tusnad and Bixad mineral compositions, respectively. [Color figure can be viewed at wileyonlinelibrary.com]

might be due to a higher residual signal because of incomplete bleaching of the post-IR $IRSL_{290}$ signal before deposition. By contrast, we cannot exclude that the OSL signal of quartz has already been saturated even though the calculated saturation level was 79 and 80%, respectively.

We obtained a maximum age of 54.8 ± 4.0 ka (Loc TUR1 in Fig. 2 from post-IR $IRSL_{290}$ measurements of sediment underlying the lower TUR tephra subunit), whereas the OSL age in the sample point between the two TUR tephra subunits in the TUR2 locality is 48.9 ± 2.9 ka. Of note, an OSL age of 48.6 ± 3.3 ka was obtained above the upper TUR tephra subunit as a minimum age of ash deposition. This age constraint places the TUR eruption in the oldest explosive phase of Ciomadul, corresponding to Eruptive episode 5/1 (Molnár *et al.*, 2019). TGS tephra occurs in all three studied localities. In the TUR1 and TUR2 outcrops, the undulated pumice layer is bracketed by ages of 31.8 ± 3.0 ka (youngest age below the TGS tephra) and 17.1 ± 0.8 ka, whereas in the TGS locality, we determined OSL ages from the samples described by Harangi *et al.* (2015) of 38.6 ± 1.9 and 31.8 ± 1.7 ka, under and above the TGS tephra layer, respectively. We also recalculated our post-IR $IRSL_{290}$ ages published by Harangi *et al.* (2015) considering no Rn escape. In this way, we obtained younger bracketing ages of 39.3 ± 3.0 and 27.0 ± 1.6 ka, which agree well with the quartz OSL ages. Combining the results in the two localities, we infer a depositional age of 31.8 ± 3.0 ka for the TGS tephra, suggesting that this large eruption could have been one of the latest in Ciomadul as inferred by Karátson *et al.* (2016) and significantly younger than proposed by Harangi *et al.* (2015).

Radiocarbon age

In the Sânmartin locality, luminescence dating was not possible, but radiocarbon dating using a two-step combustion procedure yielded an age of the palaeosol bed beneath the SNM tephra. The calibrated ^{14}C age for the combined TOC (total organic carbon; i.e. low- plus high-temperature fractions) is 35 304–33 781 cal a BP (SM_Table 10) at 0.21% carbon yield. Conventional radiocarbon ages of soil carbon fractions are often affected by reservoir effects due to contamination by groundwater carbonates that result in older ages. To obtain reliable soil burial ages, estimation of apparent ^{14}C ages of undisturbed top soils before burial is required. Due to the lack

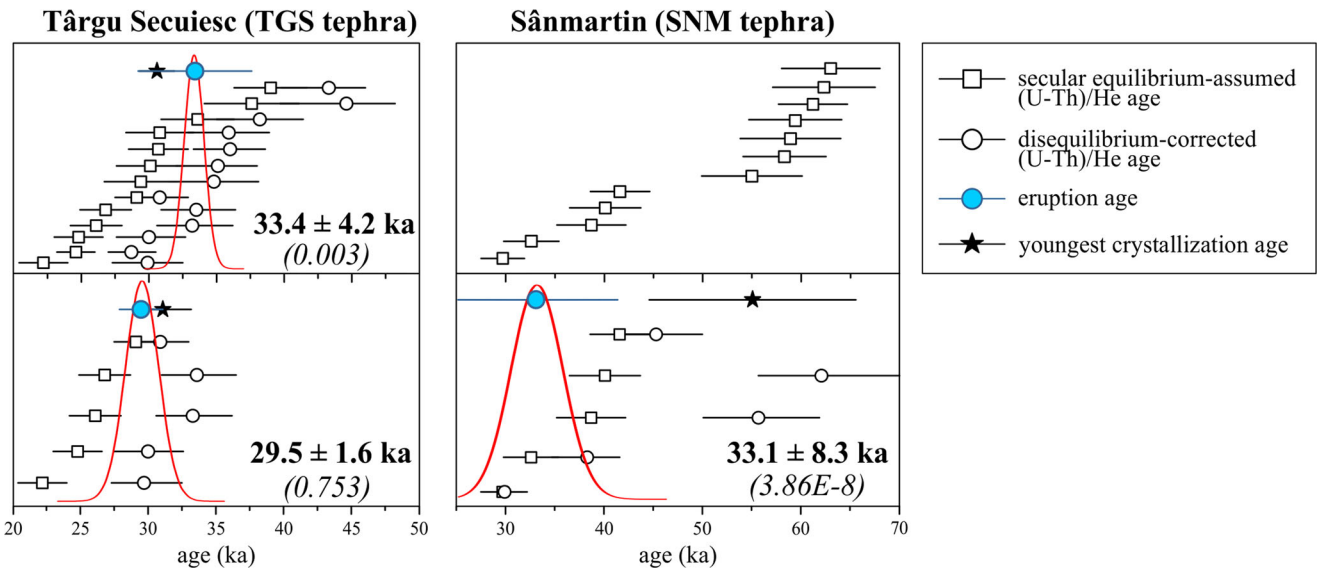

Figure 8. Disequilibrium-corrected (U-Th)/He zircon dates of single crystals and the calculated eruption age for the TGS and SNM tephras. The upper panels show results for the average crystallization age correction, whereas the lower panels show the error-weighted double-dating result. Black stars with uncertainty indicate the youngest rim age in the sample. Numbers in italic are the goodness of fit values, where the acceptable value is above 0.001 as stated by Press *et al.* (2002). [Color figure can be viewed at wileyonlinelibrary.com]

of such information, it is presently not possible to reliably estimate the reservoir effect for this palaeosol and thus the above radiocarbon age should be considered as a maximum age with the actual ages probably being a few thousand years younger.

Discussion

Eruption ages of the distal deposits

Combined zircon U-Th and (U-Th)/He dating has proved to be a powerful technique to constrain the eruption ages for Late Pleistocene to Holocene volcanic eruptions, particularly when other suitable mineral phases for dating are lacking (Schmitt *et al.*, 2006, 2010; Danišík *et al.*, 2012, 2017). Detailed eruption chronologies of the Ciomadul volcanic dome field were presented by Harangi *et al.* (2015) and Molnár *et al.* (2018, 2019) using this dating method. They pointed out that explosive volcanism occurred between 57 and 30 ka, presumably in two episodes (57–44 and 33–29 ka) in addition to lava dome extrusions. Distal volcanic deposits provide additional constraints on the explosive volcanic events even when proximal deposits have not been preserved (e.g. Shane *et al.*, 2013), as is possibly the case also for the TGS, TUR and SNM units.

New (U-Th)/He zircon dates (SM_Table 6; Fig. 8) combined with U-Th in situ rim dates of zircons presented in this paper refine the interpreted eruption age of the TGS tephra (Harangi *et al.*, 2015). In this regard, the U-Th dates of the outermost ~4-μm margin of zircon crystals have a particular relevance, because they provide an upper limit for the eruption age, i.e. the eruption must post-date the youngest crystallization age. Zircon surface ages of the TGS tephra (SM_Table 8) display a wide range of crystallization ages up to 290 ka. However, two zircon crystals gave rim ages <39 ka. Replicate rim ages on the same crystal face (30.6 ± 2.6 and 34.22 ± 6.4 ka) overlap within 2σ uncertainty and yield a maximum limit for the eruption age. Although we increased the number of zircons analysed for (U-Th)/He geochronology with respect to the work of Harangi *et al.* (2015), they still give a relatively large range of dates (F_T-corrected ages range from 113 to 22.2 ka). This can be readily explained, however, by remobilization of older volcanic material from the surface during a violent explosive eruption, when zircon from older deposits experienced only partial resetting due to limited heating (e.g. Blondes *et al.*, 2007). Thus, we omitted zircons with anomalously old (U-Th)/He dates and only considered disequilibrium-corrected dates that are coherent within analytical uncertainties. The calculated eruptive ages are younger than the age reported by Harangi *et al.* (2015) using a smaller number of zircons grains and lacking the constraint from outermost rim zircon U-Th age data. We thus favour the 29.5 ± 1.6 ka double-dating zircon age as the eruption age for the TGS tephra, because it is consistent with the youngest zircon surface ages.

This newly determined eruption age is consistent with the OSL ages published by Karátson *et al.* (2016), but the question remains why the $pIRIR_{290}$ dates of Harangi *et al.* (2015) differ? We recalculated the previously published $pIRIR_{290}$ dates considering no Rn escape. As a result, the studied sample collected above the tephra layer yielded a $pIRIR_{290}$ age of 27.0 ± 1.6 ka (after fading correction and residual subtraction) and an OSL age of 31.8 ± 1.7 ka, whereas the sample below the tephra yielded a $pIRIR_{290}$ age of 39.3 ± 3.0 ka (after residual subtraction, but without fading correction) and an OSL age of 38.6 ± 1.9 ka (SM_Table 9). These results are now closer to those published by Karátson *et al.* (2016). Furthermore, the new OSL age on quartz and the $pIRIR_{290}$ age (SM_Table 9) on feldspar from sandy sediment samples just below the undulating TGS pumice-bearing layer at the Turia quarries bracket the age of the TGS tephra within even a shorter period (31.8 ± 3 ka), which agrees well with the newly determined zircon (U-Th)/He eruption age.

The age of SNM tephra north of Ciomadul at Sânmartin was unknown due to the lack of geochronological data. Karátson *et al.* (2016) proposed that it belonged to the earliest phreatomagmatic eruption phase (EPPA) based on its glass geochemistry. The large range of the individual (U-Th)/He zircon dates (Fig. 8) is explained by incorporation of various incompletely degassed zircon grains into the eruption cloud during a phreatomagmatic eruption. However, one of these zircons has an outer rim U-Th age of 452 + ∞/−113 ka, which probably indicates secular equilibrium. Hence, the (U-Th)/He

age may not require a disequilibrium correction, and the F_T-corrected result of 29.5 ± 4.4 ka would directly represent the eruption age. This age is consistent with the radiocarbon age of the underlying palaeosol layer (<33 ka). Thus, we suggest that the explosive eruption, which produced the distal ash deposit north of Ciomadul, occurred within the youngest eruptive phase around 30 ka. Both the new TGS and the SNM ages are indistinguishable within uncertainties from the eruption age of the BIX (Bixad) tephra (32.6 ± 2 ka; Harangi *et al.*, 2015), but are different from the eruption age of the BTS (Tușnad) tephra (50.3 ± 2.6 ka; Harangi *et al.*, 2015). This indicates multiple large explosive eruptions of Ciomadul during its latest eruptive episode (29–33 ka).

Glass major element composition: does it help in eruption chronology?

Major element compositions of glass shards are widely used to correlate tephra occurrences and identify their sources (e.g. Froggatt, 1983; Stokes and Lowe, 1988; Óladóttir *et al.*, 2012; Abbott *et al.*, 2016). It is a common and powerful tool when the geochemical fingerprints of eruptive products of different volcanoes or different eruption episodes of the same volcano are known and can be clearly distinguished. This is the case in Iceland and the Mediterranean region, among others, where eruption events and/or source of the tephras can be readily identified based on the distinct major element compositions of glass shards from tephras or cryptotephras found over large distances, such as in lacustrine sediments or loess deposits (e.g. Óladóttir *et al.*, 2012; Tomlinson *et al.*, 2015).

The volcanic rocks of the Ciomadul volcanic dome field have characteristic major element compositions with relatively high-K abundances compared to the older calc-alkaline volcanic products of the nearby South Harghita volcanic chain (Fig. 2; Szakács and Seghedi, 1986; Seghedi *et al.*, 1987; Szakács *et al.*, 1993; Vinkler *et al.*, 2007; Molnár *et al.*, 2018). The glasses share the bimodal compositional character with bulk rocks (SM_Tables 1 and 2; Fig. 3). However, it is important to emphasize that the Ciomadul glasses do not represent crystal-free or crystal-poor glass shards, but the matrix of pumices and pumiceous ash fragments. Almost all glasses contain microlites (primarily plagioclase) in variable amounts that could affect the glass composition. Although this results in some intrasample compositional variation (Supporting Material_1), it does not obscure the general geochemical character of the erupted products. Glass compositions form two major groups (Figs. 3 and 5) as recognized first by Vinkler *et al.* (2007) and Harangi *et al.* (2010) who denoted them as the Bixad and Tușnad groups, respectively. This was corroborated and refined by a much larger glass compositional data set provided by Karátson *et al.* (2016). Remarkably, the mineral chemical data and the bulk rock compositions show the same bimodality, and thus there is a close correspondence between the glass (erupted melt) and bulk rock samples (erupted magma). As a consequence, the glass major element data represent well the erupted magma types.

Karátson *et al.* (2016) argued that glass major element data could be used effectively to distinguish at least three successive eruption episodes (EPPA–MPA–LSPA) of Ciomadul. This concept was used to correlate Roxolany tephra in south-western Ukraine with the youngest eruptions (LSPA) of Ciomadul (Wulf *et al.*, 2016). However, most of the LSPA glasses show a Tușnad affinity (Fig. 3). For example, glasses from tephras regarded as the youngest eruptions (boreholes in the two craters; RO-1,2,3 and SZA-2013) cannot be compositionally distinguished from the Tușnad group, whereas the uppermost tephra at the Bolondos locality (BOL-1 in Karátson *et al.*, 2016) has a Bixad affinity. In fact, there are only a few samples having heterogeneous glass compositions falling between the two main groups. In this regard, the application of glass composition as a tephrostratigraphic tool is highly questionable, and the presence of LSPA tephra at the Roxolany location cannot be validated. We show here that glass compositions, equivalent to bulk rock data, represent two main erupted magma types and that there is no systematic compositional variation in the glass composition with time. In turn, eruption of these two main magmas occurred repeatedly during the 57–30 ka eruptive epoch of Ciomadul with its mostly explosive eruptions (Fig. 9). Furthermore, during the youngest eruption stage (33–29 ka), both magma types can be recognized in the glass compositions. Thus, major element compositions of Ciomadul glasses alone cannot be used to distinguish single eruption events, but they may be useful to identify the Ciomadul source during its eruption epoch between 57 and 30 ka.

The Ciomadul tephra in the Mediterranean tephrochronology

Late Pleistocene tephras derived by large explosive volcanic eruptions are widespread in the Mediterranean and surrounding areas and they are used as important isochronous markers in stratigraphic sections (Tomlinson *et al.*, 2012a, 2015). The recognized ages of these tephra layers provide fundamental information for correlation between terrestrial and marine archives and these data are used in palaeoclimatology and archaeology (Lowe, 2011). Tomlinson *et al.* (2015) compiled a large electron microprobe glass data set from proximal tephra deposits of large explosive eruptions in the central and western Mediterranean for the last 100 kyr. Recognition of the young (57–30 ka), mostly explosive volcanism of Ciomadul adds a further potential source for tephras in the eastern Mediterranean. Harangi et al (2015) deduced that some of the 60–40 ka cryptotephra layers with an unknown origin in a drilling core from the south-east Black Sea could have been derived from

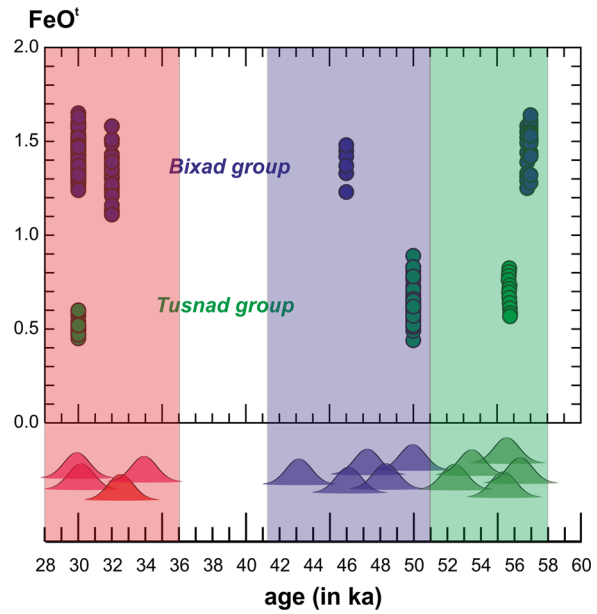

Figure 9. Eruption ages (shown in the lower panel with probability density curves from Molnár *et al.*, 2019) vs. FeO^t in glass (data are from Karátson *et al.*, 2016 and this study). Note absence of systematic changes in erupted melt/magma composition with time. Magmas with Tușnad- and Bixad-type affinity erupted repeatedly and are occasionally coeval. [Color figure can be viewed at wileyonlinelibrary.com]

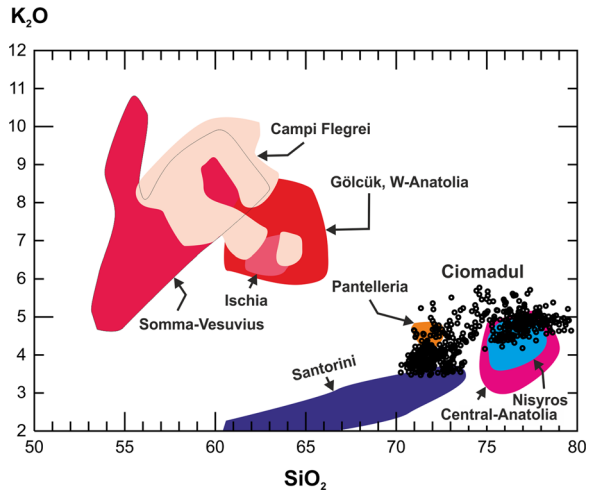

Figure 10. SiO_2 vs. K_2O (wt%) plot for glasses of various Quaternary explosive eruption products in the Mediterranean region (Tomlinson *et al.*, 2012a,b, 2015) compared to glass data of Ciomadul pumice (Vinkler *et al.*, 2007; Karátson *et al.*, 2016; this study). Note the bimodal character of the Ciomadul glasses. [Color figure can be viewed at wileyonlinelibrary.com]

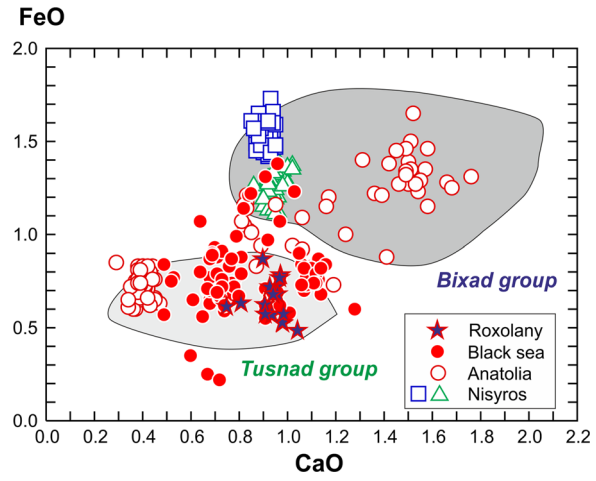

Figure 11. CaO vs. FeO abundances (wt%) in glasses of Ciomadul (presented as Bixad and Tușnad group; see Fig. 3), Nisyros and Anatolian tephras (Tomlinson *et al.*, 2012a, 2015). For comparison, glass compositions of >30-ka cryptotephras of the Black Sea drill core (Campanian ignimbrite tephra is excluded; Cullen *et al.*, 2014) and Roxolany tephra, which was correlated with Ciomadul by Wulf *et al.* (2016), are shown. [Color figure can be viewed at wileyonlinelibrary.com]

Ciomadul, whereas Wulf *et al.* (2016) suggested that the Roxolany tephra at the north-western margin of the Black Sea (Fig. 1) could be also one of the latest eruption products of Ciomadul.

The major element compositions of the Ciomadul glasses (SM_Table 2) differ significantly from those of Neapolitan volcanoes. The rhyolitic composition along with the eruption dates are, however, close to that of the 45.7-ka Green tuff, Pantelleria (Karkanas *et al.*, 2015; Tomlinson *et al.*, 2015), the 47-ka Upper Pumices from Nisyros (Tomlinson *et al.*, 2012b) and some of the volcanic products from Central Anatolia (Kuzucuoglu *et al.*, 1998; Tomlinson *et al.*, 2015; Fig. 10). Tephras from Roxolany (Wulf *et al.*, 2016) and from Black Sea drill cores (Cullen *et al.*, 2014) also have similar glass compositions. Using various bivariate major element plots, the Pantellerian Green tuff can be readily distinguished based on its high FeO content, which differs from other tephras. In turn, the Nisyros Upper Pumice glasses and many of the Anatolian tephras have overlapping major element content with the Ciomadul glasses. Remarkably, the Black Sea and Roxolany tephras resemble only the Tușnad group of the Ciomadul glasses (Fig. 11).

At this stage, we conclude that glass major element composition is not necessarily discriminative of certain volcanic sources and events in the Mediterranean and surrounding regions. This is quite common worldwide, when major elements in glasses alone cannot discriminate eruption events (Izett *et al.*, 1988; Perkins and Nash, 2002; Pearce *et al.*, 2008, 2014; Westgate *et al.*, 2013). The petrological reason for this is primarily that similar eutectic/minimum compositions are reached by evolved rhyolitic melts even though they had different magma differentiation paths and possibly different parental magmas. In contrast, trace element abundances of evolved melts could vary considerably, as they are controlled by crystal/melt partitioning. Furthermore, investigating the characteristic mineral cargo of the erupted magma can be another tool to distinguish tephra deposits having similar major element composition.

Fingerprinting the Ciomadul tephra

Given that major elements in glasses alone often result in ambiguous results for tephra provenance, Lowe (2011) emphasized that multiple criteria should be used for that purpose. In addition to major elements, glass texture and morphology, mineral assemblage and trace element abundances could provide unique tephra fingerprints. In the following, we use other methods in addition to the already described glass major element compositions to characterize the 57–30 ka Ciomadul tephra.

Ciomadul explosive volcanic products have a typical phenocryst assemblage containing plagioclase, amphibole (hornblende and pargasite) and biotite. In this regard, the Roxolany tephra differs significantly from Ciomadul, as it contains clinopyroxene (Wulf *et al.*, 2016) instead of amphibole. Clinopyroxene is very rare in Ciomadul dacites and if it occurs it is magnesium-rich (Mg-number is typically >85) and often surrounded by amphibole. It is found mostly in the lava dome rocks and rarely in explosive volcanic products. Thus, the clinopyroxene-bearing Roxolany tephra is unlikely to be derived from Ciomadul. Mineral compositions can be also used to fingerprint Ciomadul tephra (Fig. 7). There is a subtle but significant bimodality in the two magma types identified by glass chemistry. Eruption products of the Tușnad group (e.g. 50-ka Tușnad pumice, 50-ka TUR ash at Turia, 33–30-ka SNM ash at Sânmartin) contain plagioclase with lower An content (typically between 25 and 35 mol%) and amphiboles with lower Al_2O_3 (<9 wt%), compared to the Bixad group rocks (e.g. 57-ka Bolondos lower pumice, 32-ka Bixad pumice and 30-ka TGS pumice; plagioclases: typically 40–50 mol% An content; amphiboles: Al_2O_3 > 10 wt%). Furthermore, amphibole in Ciomadul dacite usually displays complex zoning with hornblende and pargasitic compositions even within single crystals (Kiss *et al.*, 2014), which is typical for both the Tusnad and the Bixad groups and could be a characteristic fingerprint for tephra derived from Ciomadul.

Ciomadul dacite has a distinctive trace element feature (Seghedi *et al.*, 1987; Szakács *et al.*, 1993; Mason *et al.*, 1996; Vinkler *et al.*, 2007; Molnár *et al.*, 2018, 2019) showing enrichment in Ba and Sr (>1000 p.p.m. for both elements) and concomitant depletion in Y and HREE (Y<17 p.p.m.; Yb<1.8 p.p.m.; La/Yb>30). This separates them clearly from the older (>1.5 Ma) calc-alkaline rocks of South Harghita (Mason *et al.*, 1996; Molnár *et al.*, 2018). Matrix glass trace element compositions analysed by LA-ICP-MS (SM_Table 3) are similar to bulk rock compositions, suggesting that both bulk pumice and in situ glass data can characterize the Ciomadul source

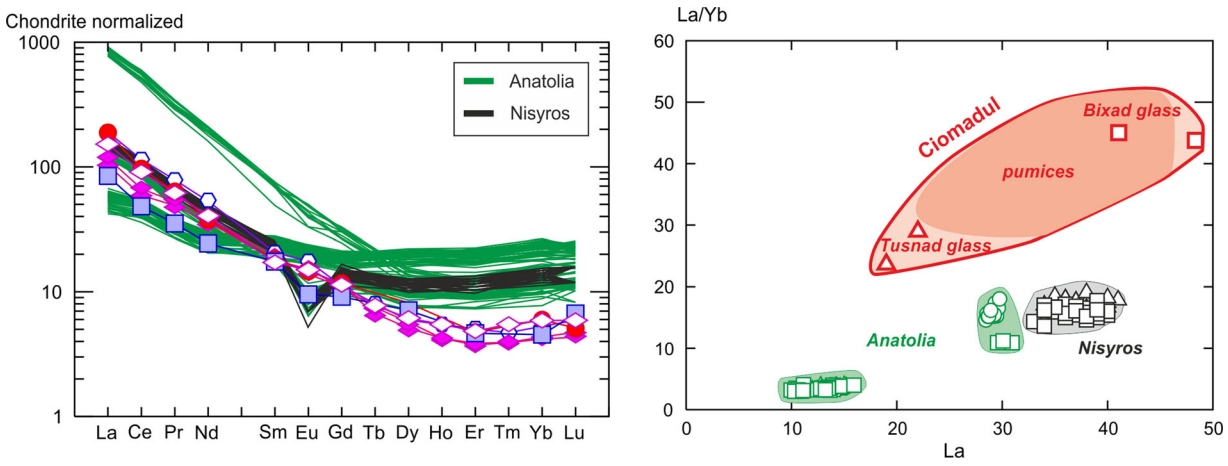

Figure 12. Trace element abundances (p.p.m.) of Ciomadul tephras (symbols as in Fig. 11). Ciomadul tephras can be readily distinguished from Anatolian and Nisyros tephras (data from Tomlinson *et al.*, 2012a, 2015), which have similar major element compositions. [Color figure can be viewed at wileyonlinelibrary.com]

(Fig. 6). The Bixad and Tușnad groups differ subtly, where the former has slightly higher light rare-earth element abundances and therefore higher La/Yb compared to the Tușnad group. Using this trace element fingerprint, Ciomadul tephras can be readily distinguished from tephras having similar major element composition such as those derived from Anatolian volcanoes or Nisyros (Fig. 12).

Conclusions

In this study we demonstrate that multiple criteria involving precise geochronological data, petrological and geochemical fingerprinting of volcanic products can be effectively used to characterize the distinctive features of a volcano and/or a volcanic eruption and correlate distal tephras with their source volcanoes. (U-Th)/He zircon geochronology combined with U-Th in situ rim dating is a powerful tool to determine the eruption ages of Late Pleistocene tephras. Using this methodology and complementing it with luminescence and radiocarbon dating, we could constrain the eruption ages of the largest explosive eruptions of Ciomadul that yielded distal tephra layers, but no preserved proximal deposits. Petrological and geochemical fingerprinting of the Ciomadul volcanic products could help in constraining the tephrochronology in the eastern Mediterranean region. The specific petrological character (ash texture, occurrence of plagioclase and amphibole phenocrysts and their compositions), the major element composition and particularly the distinctive trace element characteristics are a fingerprint for Ciomadul tephras that can be used for correlating tephra and cryptotephra occurrences in the Mediterranean within the timeframe of 57–30 ka. We also showed that glass major element compositions are often ambiguous regarding the eruption source, particularly in the case of calc-alkaline dacitic to rhyolitic magmas. However, glass trace elements as well as the mineral cargo can be effectively used to find the origin of such tephras.

Supporting information

Additional supporting information may be found in the online version of this article at the publisher's web-site.
Material 1. Methods (PDF)
Material 2. Volcanological description of the distal sections along with IRSL dating results (PDF)
Material 3. Data tables (XLS)
SM_Table 1. Bulk rock composition of the studied tephra and representative proximal pumice samples from Ciomadul
SM_Table 2. Major element composition of glasses of the studied tephras
SM_Table 3. LA-ICP-MS trace element composition of pumice glasses from Tusnad and Bixad localities
SM_Table 4. Composition of plagioclases in the studied Ciomadul tephra deposits (Ab – albite, An – anorthite, Or – orthoclase end-members in mol%)
SM_Table 5. Composition of amphiboles in the studied Ciomadul tephra deposits (Al^{iv} – tetrahedral Al; mg-value: $Mg^{2+}/(Mg^{2+} + Fe^{2+})$)
SM_Table 6. (U-Th)/He zircon dates and calculated eruption ages
SM_Table 7. (U-Th)/He zircon double dating ages
SM_Table 8. U-Th zircon model dates
SM_Table 9. Luminescence dating of the sediments comprising the TUR and TGS tephras
SM_Table 10. Radiocarbon dating of the palaeosoil beneath the SNM tephra

Acknowledgements. This study is part of the research project supported by the Hungarian National Research, Development and Innovation Fund (NKFIH) within No. K116528 and PD 121048. This work was partly supported by the European Union and the State of Hungary, co-financed by the European Regional Development Fund within the GINOP-2.3.2-15-2016-00009 'ICER' project. I. Seghedi benefited from a grant of the Ministry of Research and Innovation, CNCS–UEFISCDI, project no. PN-III-P4-ID-PCCF-2016-4-0014, within PNCDI III, while B. Kiss's work was supported by the Hungarian National Research, Development and Innovation Fund (NKFIH) within no. PD 130214. Constructive comments provided by Lorenzo Fedele and an anonymous reviewer as well as by Daniel Veres, as guest editor, helped us to clarify our ideas.

Abbreviations. BIX, Bixad; EPPA, Early Phreatomagmatic and Plinian Activity; HREE, heavy rare earth element; LA-ICP-MS, laser-ablation inductively coupled plasma mass spectrometry; LSPA, Latest St. Ana Phreatomagmatic Activity; MPA, Middle Plinian Activity; OSL, optically stimulated luminescence; post-IR $IRSL_{290}$, post-IR infra-red stimulated luminescence; TOC, total organic carbon.

References

Abbott PM, Bourne AJ, Purcell CS, *et al.* 2016. Last glacial period cryptotephra deposits in an eastern North Atlantic marine sequence: exploring linkages to the Greenland ice-cores. *Quaternary Geochronology* **31**: 62–76. https://doi.org/10.1016/j.quageo.2015.11.001

Blockley SPE, Pyne-O'Donnell SDF, Lowe JJ, *et al.* 2005. A new and less destructive laboratory procedure for the physical separation of distal glass tephra shards from sediments. *Quaternary Science*

Reviews **24**: 1952–1960. https://doi.org/10.1016/j.quascirev.2004.12.008

Blondes MS, Reiners PW, Edwards BR, *et al*. 2007. Dating young basalt eruptions by (U-Th)/He on xenolithic zircons. *Geology* **35**: 17–20. https://doi.org/10.1130/G22956A.1

Bosio G, Gioncada A, Malinverno E, *et al*. 2019. Chemical and petrographic fingerprinting of volcanic ashes as a tool for high-resolution stratigraphy of the Upper Miocene Pisco Formation (Peru). *Journal of the Geological Society* **176**: 13–28. https://doi.org/10.1144/jgs2018-071

Bouvet de Maisonneuve C, Bachmann O, Burgisser A. 2009. Characterization of juvenile pyroclasts from the Kos Plateau Tuff (Aegean Arc): insights into the eruptive dynamics of a large rhyolitic eruption. *Bulletin of Volcanology* **71**: 643–658. https://doi.org/10.1007/s00445-008-0250-x

Cullen VL, Smith VC, Arz HW. 2014. The detailed tephrostratigraphy of a core from the south-east Black Sea spanning the last ~60 ka. *Journal of Quaternary Science* **29**: 675–690. https://doi.org/10.1002/jqs.2739

Danišík M, Schmitt AK, Stockli DF, *et al*. 2017. Application of combined U-Th-disequilibrium/U-Pb and (U-Th)/He zircon dating to tephrochronology. *Quaternary Geochronology* **40**: 23–32. https://doi.org/10.1016/j.quageo.2016.07.005

Danišík M, Shane P, Schmitt AK, *et al*. 2012. Re-anchoring the late Pleistocene tephrochronology of New Zealand based on concordant radiocarbon ages and combined $^{238}U/^{230}Th$ disequilibrium and (U–Th)/He zircon ages. *Earth and Planetary Science Letters* **349–350**: 240–250. https://doi.org/10.1016/j.epsl.2012.06.041

Davies SM. 2015. Cryptotephras: the revolution in correlation and precision dating. *Journal of Quaternary Science* **30**: 114–130. https://doi.org/10.1002/jqs.2766]

de Silva SL, Francis PW. 1989. Correlation of large ignimbrites – two case studies from the Central Andes of northern Chile. *Journal of Volcanology and Geothermal Research* **37**: 133–149. https://doi.org/10.1016/0377-0273(89)90066-8

Farley KA, Kohn BP, Pillans B. 2002. The effects of secular disequilibrium on (U–Th)/He systematics and dating of Quaternary volcanic zircon and apatite. *Earth and Planetary Science Letters* **201**: 117–125. https://doi.org/10.1016/S0012-821X(02)00659-3

Froggatt PC. 1983. Toward a comprehensive upper quaternary tephra and ignimbrite stratigraphy in New Zealand using electron microprobe analysis of glass shards. *Quaternary Research* **19**: 188–200. https://doi.org/10.1016/0033-5894(83)90004-2

Harangi S, Lukács R, Schmitt AK, *et al*. 2015. Constraints on the timing of Quaternary volcanism and duration of magma residence at Ciomadul volcano, east–central Europe, from combined U–Th/He and U–Th zircon geochronology. *Journal of Volcanology and Geothermal Research* **301**: 66–80. https://doi.org/10.1016/j.jvolgeores.2015.05.002

Harangi S, Mason PRD, Lukács R. 2005. Correlation and petrogenesis of silicic pyroclastic rocks in the northern Pannonian Basin, Eastern–Central Europe: in situ trace element data of glass shards and mineral chemical constraints. *Journal of Volcanology and Geothermal Research* **143**: 237–257. https://doi.org/10.1016/j.jvolgeores.2004.11.012

Harangi Sz, Molnár M, Vinkler AP, *et al*. 2010. Radiocarbon dating of the last volcanic eruptions of Ciomadul volcano, Southeast Carpathians, eastern–central Europe. *Radiocarbon* **52**: 1498–1507. https://doi.org/10.1017/S0033822200046580

Izett GA, Obradovich JD, Mehnert HH. 1988. The Bishop ash bed (Middle Pleistocene) and some older (Pliocene and Pleistocene) chemically and mineralogically similar ash beds in California, Nevada, and Utah. *USGS Bulletin* **1675**.

Karátson D, Telbisz T, Dibacto S, *et al*. 2019. Eruptive history of the Late Quaternary Ciomadul (Csomád) volcano, East Carpathians, Part II: magma output rates. *Bulletin of Volcanology* **81**: 28. https://doi.org/10.1007/s00445-019-1287-8

Karátson D, Wulf S, Veres D, *et al*. 2016. The latest explosive eruptions of Ciomadul (Csomád) volcano, East Carpathians – A tephrostratigraphic approach for the 51–29ka BP time interval. *Journal of Volcanology and Geothermal Research* **319**: 29–51. https://doi.org/10.1016/j.jvolgeores.2016.03.005

Karkanas P, White D, Lane CS, *et al*. 2015. Tephra correlations and climatic events between the MIS6/5 transition and the beginning of MIS3 in Theopetra Cave, central Greece. *Quaternary Science Reviews* **118**: 170–181. https://doi.org/10.1016/j.quascirev.2014.05.027

Kiss B, Harangi S, Ntaflos T, *et al*. 2014. Amphibole perspective to unravel pre-eruptive processes and conditions in volcanic plumbing systems beneath intermediate arc volcanoes: a case study from Ciomadul volcano (SE Carpathians). *Contributions to Mineralogy and Petrology* **167**: 986. https://doi.org/10.1007/s00410-014-0986-6

Kuzucuoglu C, Pastre J-F, Black S, *et al*. 1998. Identification and dating of tephra layers from Quaternary sedimentary sequences of Inner Anatolia, Turkey. *Journal of Volcanology and Geothermal Research* **85**: 153–172. https://doi.org/10.1016/S0377-0273(98)00054-7

Lahitte P, Dibacto S, Karátson D, *et al*. 2019. Eruptive history of the Late Quaternary Ciomadul (Csomád) volcano, East Carpathians, Part I: timing of lava dome activity. *Bulletin of Volcanology* **81**: 27. https://doi.org/10.1007/s00445-019-1286-9

Lowe DJ. 2011. Tephrochronology and its application: a review. *Quaternary Geochronology* **6**: 107–153. https://doi.org/10.1016/j.quageo.2010.08.003

Mason PRD, Downes H, Thirlwall MF, *et al*. 1996. Crustal assimilation as a major petrogenetic process in the east Carpathian Neogene and Quaternary continental margin arc, Romania. *Journal of Petrology* **37**: 927–959. https://doi.org/10.1093/petrology/37.4.927

Molnár K, Harangi S, Lukács R, *et al*. 2018. The onset of the volcanism in the Ciomadul Volcanic Dome Complex (Eastern Carpathians): eruption chronology and magma type variation. *Journal of Volcanology and Geothermal Research* **354**: 39–56. https://doi.org/10.1016/j.jvolgeores.2018.01.025

Molnár K, Lukács R, Dunkl I, *et al*. 2019. Episodes of dormancy and eruption of the Late Pleistocene Ciomadul volcanic complex (Eastern Carpathians, Romania) constrained by zircon geochronology. *Journal of Volcanology and Geothermal Research* **373**: 133–147. https://doi.org/10.1016/j.jvolgeores.2019.01.025

Óladóttir BA, Larsen G, Sigmarsson O. 2012. Deciphering eruption history and magmatic processes from tephra in Iceland. *Jökull* **62**: 21–38.

Pearce NJG, Alloway BV, Westgate JA. 2008. Mid-Pleistocene silicic tephra beds in the Auckland region, New Zealand: their correlation and origins based on the trace element analyses of single glass shards. *Quaternary International* **178**: 16–43. https://doi.org/10.1016/j.quaint.2006.09.005

Pearce NJG, Denton JS, Perkins WT, *et al*. 2007. Correlation and characterisation of individual glass shards from tephra deposits using trace element laser ablation ICP-MS analyses: current status and future potential. *Journal of Quaternary Science* **22**: 721–736. https://doi.org/10.1002/jqs.1092

Pearce NJG, Westgate JA, Gatti E, *et al*. 2014. Individual glass shard trace element analyses confirm that all known Toba tephra reported from India is from the c. 75-ka Youngest Toba eruption. *Journal of Quaternary Science* **29**: 729–734. https://doi.org/10.1002/jqs.2741

Pearce NJG, Westgate JA, Perkins WT, *et al*. 1999. The application of laser ablation ICP-MS to the analysis of volcanic glass shards from tephra deposits: bulk glass and single shard analysis. *Global and Planetary Change* **21**: 151–171. https://doi.org/10.1016/S0921-8181(99)00012-0

Perkins ME, Nash BP. 2002. Explosive silicic volcanism of the Yellowstone hotspot: the ash fall tuff record. *Geological Society of America Bulletin* **114**: 367–381. https://doi.org/10.1130/0016-7606(2002)114<0367:ESVOTY>2.0.CO;2

Press WH, Teukolsky SA, Vetterling WT, *et al*. 2002. *Numerical Recipes: the Art of Scientific Computing*. Cambridge University Press: Cambridge.

Schmitt AK, Stockli DF, Hausback BP. 2006. Eruption and magma crystallization ages of Las Tres Vírgenes (Baja California) constrained by combined $^{230}Th/^{238}U$ and (U–Th)/He dating of zircon. *Journal of Volcanology and Geothermal Research* **158**: 281–295. https://doi.org/10.1016/j.jvolgeores.2006.07.005

Schmitt AK, Stockli DF, Niedermann S, *et al*. 2010. Eruption ages of Las Tres Vírgenes volcano (Baja California): a tale of two helium isotopes. *Quaternary Geochronology* **5**: 503–511.

Seghedi I, Szakács A, Udrescu C, *et al*. 1987. Trace element geochemistry of the South Hargitha volcanics (East Carpathians): calc-alkaline and shoshonitic association. *Dari de Seama ale Sedintelor Institutul de Geologie și Geofizica* **72–73**: 381–397.

Shane P. 2000. Tephrochronology: a New Zealand case study. *Earth-Science Reviews* **49**: 223–259. https://doi.org/10.1016/S0012-8252(99)00058-6

Shane P, Gehrels M, Zawalna-Geer A, *et al*. 2013. Longevity of a small shield volcano revealed by crypto-tephra studies (Rangitoto volcano, New Zealand): change in eruptive behavior of a basaltic field. *Journal of Volcanology and Geothermal Research* **257**: 174–183. https://doi.org/10.1016/j.jvolgeores.2013.03.026

Shane P, Smith V, Nairn I. 2003. Biotite composition as a tool for the identification of Quaternary tephra beds. *Quaternary Research* **59**: 262–270. https://doi.org/10.1016/S0033-5894(03)00012-7

Stokes S, Lowe DJ. 1988. Discriminant function analysis of late Quaternary tephras from five volcanoes in New Zealand using glass shard major element chemistry. *Quaternary Research* **30**: 270–283. https://doi.org/10.1016/0033-5894(88)90003-8

Sun S-s, McDonough WF. 1989. Chemical and isotopic systematics of oceanic basalts: implications for mantle composition and processes. *Geological Society, London, Special Publications* **42**: 313–345. https://doi.org/10.1144/GSL.SP.1989.042.01.19

Szakács A, Seghedi I. 1986. Chemical diagnosis of the volcanics from the southeasternmost part of the Harghita Mountains – proposal for a new nomenclature. *Revue Roumaine de Géologie* **30**: 41–48.

Szakács A, Seghedi I, Pécskay Z. 1993. Peculiarities of South Harghita Mts. as terminal segment of the Carpathian Neogene to Quaternary volcanic chain. *Revue Roumaine de. Geologie* **37**: 21–36.

Szakács A, Seghedi I, Pécskay Z, *et al*. 2015. Eruptive history of a low-frequency and low-output rate Pleistocene volcano, Ciomadul, South Harghita Mts., Romania. *Bulletin of Volcanology* **77**: 12. https://doi.org/10.1007/s00445-014-0894-7

Tomlinson EL, Arienzo I, Civetta L, *et al*. 2012a. Geochemistry of the Phlegraean Fields (Italy) proximal sources for major Mediterranean tephras: implications for the dispersal of Plinian and co-ignimbritic components of explosive eruptions. *Geochimica et Cosmochimica Acta* **93**: 102–128. https://doi.org/10.1016/j.gca.2012.05.043

Tomlinson EL, Kinvig HS, Smith VC, *et al*. 2012b. The Upper and Lower Nisyros Pumices: revisions to the Mediterranean tephrostratigraphic record based on micron-beam glass geochemistry. *Journal of Volcanology and Geothermal Research* **243–244**: 69–80. https://doi.org/10.1016/j.jvolgeores.2012.07.004

Tomlinson EL, Smith VC, Albert PG, *et al*. 2015. The major and trace element glass compositions of the productive Mediterranean volcanic sources: tools for correlating distal tephra layers in and around Europe. *Quaternary Science Reviews* **118**: 48–66. https://doi.org/10.1016/j.quascirev.2014.10.028

Tomlinson EL, Thordarson T, Müller W, *et al*. 2010. Microanalysis of tephra by LA-ICP-MS – strategies, advantages and limitations assessed using the Thorsmörk ignimbrite (Southern Iceland). *Chemical Geology* **279**: 73–89. https://doi.org/10.1016/j.chemgeo.2010.09.013

Veres D, Cosac M, Schmidt C, *et al*. 2018. New chronological constraints for Middle Palaeolithic (MIS 6/5–3) cave sequences in Eastern Transylvania, Romania. *Quaternary International* **485**: 103–114. https://doi.org/10.1016/j.quaint.2017.07.015

Vinkler AP, Harangi S, Ntaflos T, *et al*. 2007. A Csomád vulkán (Keleti-Kárpátok) horzsaköveinek kőzettani és geokémiai vizsgálata – petrogenetikai következtetések. *Földtani Közlöny* **137**: 103–128.

Westgate JA, Pearce NJG, Perkins WT, *et al*. 2013. Tephrochronology of the Toba tuffs: four primary glass populations define the 75-ka Youngest Toba Tuff, northern Sumatra, Indonesia. *Journal of Quaternary Science* **28**: 772–776. https://doi.org/10.1002/jqs.2672

Wulf S, Fedorowicz S, Veres D, *et al*. 2016. The 'Roxolany Tephra' (Ukraine) – new evidence for an origin from Ciomadul volcano, East Carpathians. *Journal of Quaternary Science* **31**: 565–576. https://doi.org/10.1002/jqs.2879

Wulf S, Hardiman MJ, Staff RA, *et al*. 2018. The marine isotope stage 1–5 cryptotephra record of Tenaghi Philippon, Greece: towards a detailed tephrostratigraphic framework for the eastern Mediterranean region. *Quaternary Science Reviews* **186**: 236–262. https://doi.org/10.1016/j.quascirev.2018.03.011

